Towards a unified model-free control architecture for tailsitter micro air vehicles: Flight simulation analysis and experimental flights

Jacson Miguel Olszanecki Barth, Jean-Philippe Condomines, Murat Bronz, Gautier Hattenberger, Jean-Marc Moschetta, Cédric Join, Michel Fliess

Towards a Unified Model-Free Control Architecture for Tail Sitter Micro Air Vehicles: Flight Simulation Analysis and Experimental Flights

Jacson Miguel Olszanecki Barth*, Jean-Philippe Condomines†, Murat Bronz‡, Gautier Hattenberger§
ENAC, Université de Toulouse, 31055, France

Jean-Marc Moschetta¶
Institut Supérieur de l'Aéronautique et de l'Espace, Toulouse, 31400, France

Cédric Join‖
Université de Lorraine, Vandœuvre-lès-Nancy, 54506, France

Michel Fliess**
École polytechnique, Palaiseau, 91128, France

Hybrid Micro Air Vehicles (MAVs) combine the beneficial features of rotorcrafts with fixed-wing configurations providing a complete flight envelope that includes vertical take-off, hovering, transitioning flights, forward flight and vertical landing. Tail sitter MAVs belong to a particular class of hybrid MAVs and its peculiar issue is related to the transitioning flight phase where, for high incidence angles, fast changing of aerodynamic forces and moments are observed which are difficult to model and control accurately. To overcome this issue, we propose a control architecture with model-free control algorithms that is able to stabilize the hybrid MAV's attitude, velocity, and position without any modeling process. The proposed control architecture consists basically on two steps : 1) The attitude control, in order to ensure the hybrid MAV's attitude orientation and stability during the entire flight envelope; 2) The guidance system responsible to control both velocity and position. We validate the MFC architecture according to a comprehensive set of flight simulations and real flight experiments. Real flight experiments shown an effective and promising control strategy solving the principal issue of hybrid MAVs that is the formulation of accurate hybrid MAV's dynamic equations to design control laws. The obtained results provide a straightforward way to validate the methodological principles presented in this article as well as certify the designed MFC parameters, and establish a conclusion regarding MFC benefits in both theoretical and practical contexts.

I. Introduction

Over the last decades, aerospace engineers have contributed to the design of different Micro Air Vehicle (MAV) configurations proposing innovative solutions for complex flight missions in outdoor or indoor environments. Recent advances in embedded systems which include sensors miniaturization and faster microprocessors allowing high frequency processes for on board computing operations brought together high flight performance demands which imply, for each flight mission, the assignment of an appropriated MAV configuration. For long endurance flight missions, the use of fixed-wing configurations is suitable due to their optimized aerodynamic surfaces that, in contact with mass of air in mouvement, generate lift force relieving the energy consumption. On the other hand, in terms of flight

*Ph.D. Candidate, ENAC, Université de Toulouse, e-mail:jacson-miguel.olszanecki-barth@enac.fr; AIAA Student Member
†Assistant Professor, ENAC, Université de Toulouse, e-mail:jean-philippe.condomines@enac.fr
‡Assistant Professor, ENAC, Université de Toulouse, Drones Research Group, e-mail:murat.bronz@enac.fr
§Assistant Professor, ENAC, Université de Toulouse, e-mail:gautier.hattenberger@enac.fr
¶Professor, ISAE-SUPAERO, Department of Aerodynamics, Energetics and Propulsion, e-mail:jean-marc.moschetta@isae-supaero.fr
‖Professor, Université de Lorraine, CRAN (CNRS, UMR 7039) & AL.I.E.N (ALgèbre pour Identification Estimation Numérique), 54330 Vézelise, France, e-mail:cedric.join@univ-lorraine.fr
**Professor, École polytechnique, LIX (CNRS, UMR 7161) & AL.I.E.N (ALgèbre pour Identification Estimation Numérique), 54330 Vézelise, France, e-mail:Michel.Fliess@polytechnique.edu

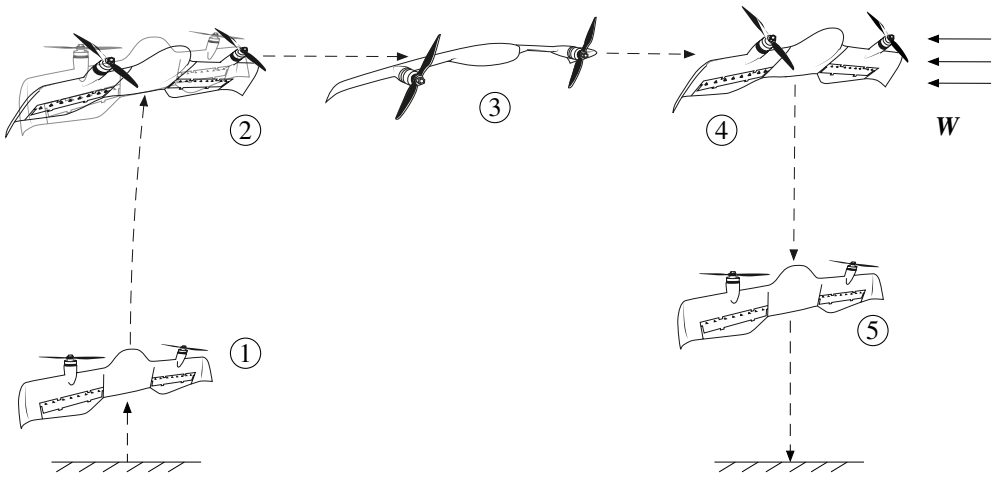

Fig. 1 Typical flight modes of Tail Sitter Micro Air Vehicles: 1 - Vertical take-off; 2 - Transitioning flight; 3 - Forward flight; 4 - Hovering flight; 5 - Vertical landing. The vector *W* represents the wind disturbances.

maneuverability, rotorcraft are preferred due to their hovering flight capabilities that enable vertical take-off and landing, as well as stationary flights. However, their energetically expensive propulsion system is not viable for long endurance flights. For missions that demand the combination of endurance and maneuverability features, structural aerodynamic engineers developed the so-called hybrid MAVs that operate over a wide flight envelope including vertical take-off, efficient forward flight, transitioning flights, hovering, and vertical landing according to Fig. 1. While these different flight aptitudes enlarge its application range, aerodynamic optimization of the MAV cell must be led by aerodynamic designers considering the challenges of each flight domain. Furthermore, the autopilot system must ensure the stability and the tracking trajectories for the entire flight envelope considering the particularities of each flight domain and also the interactions between them which results a higher degree of challenge and complexity also for the guidance, navigation, and control community. Different hybrid MAV configurations can be found in the literature, such as tilt rotors [1] or tilt wings [2], quadplanes [3], and tilt body or tail sitter [4]. These platforms have been designed in order to solve the aerodynamic and mechanical limitations of each of them and the choice of the appropriated MAV configuration varies according to the imposed flight mission specifications. For instance, maximum payload, the desired endurance, the range and the inherent stability against the windy environment. Generally, tail sitter MAVs are designed and optimized to perform an efficient forward flight, since this flight phase represents most of its mission. Various studies have improved and assessed the aerodynamic properties of MAVs previously [5] [6]. However, the flap effectiveness needs to be optimized in order to create sufficient pitch moment ensuring the control authority during the transitioning flights. We focalize our research work in the design and control of tail sitter MAVs investigating the performance of this peculiar MAV class for three reasons : 1) Tail sitter are more enduring in forward flight when we compare to others; 2) The simple transition mechanisms, in relation to tilt rotors that need additional actuators to orientate the propeller in order to perform the transitioning flight; 3) The challenge of attitude stabilization during hovering and transitioning flights in windy conditions. Tail sitter are susceptible to wind disturbances during these flight phases, its stabilization remains an attractive, motivating and challenging control research topic. Typically, its entire flight envelope can be analysed in three distinct flight modes, namely, hovering flight, forward flight and transitioning flight. While hovering and forward flights were well researched and can be studied using a linearized system around an equilibrium point facilitating the impementation of classical linear control algorithms. The transition flight possesses some peculiarities that includes fast changing of aerodynamic forces and moments with wing behaviours partially stalled. Based on such aerodynamic effects, a reliable model that accurately represent the flight dynamics of a tail sitter MAVs over their entire flight envelope remains expensive, time consuming and a difficult task. Due to these practical modeling issues, some research works considered the transition flight as an undesirable and transient flight phase. However, we can not neglect the fact that, transitioning phase needs to be continuously stabilized in order to ensure a smooth and safe flight, especially against wind disturbances. Tail sitter MAV model is often considered by the control community as a parameter-varying system, e.g. the change of aerodynamic coefficients according to its attitude orientation and the environmental wind conditions. Consequently, design a control technique for autopilot systems that does not rely on

prior knowledge of tail sitter MAV model becomes an intuitive, inovative and, from the point of view of the authors, an appropriate control methodology. Therefore, the development of a such controller that estimates the tail sitter MAV dynamics and counteracts it, in real time, can be easily adaptable and implemented for different hybrid MAVs.

A. Control literature review

Different control strategies have been designed for hybrid MAVs, we present some of them in the following with particular emphasis in the controllers developed for the tail-sitter class. For practical reasons, classical linear controllers designed using PID techniques have been used in some works [7] [8]. Although simple to tune without the knowledge of the controlled system dynamics, PID controllers are known by the lack of robustness against significant wind disturbances. Autopilot systems develop from optimal control theory, have been researched. For instance, the Linear Quadratic Regulator (LQR) which was designed and applied for a tail-sitter MAV previously modelized and identified from wind tunnel campaign [9]. The performance of model-based controllers differs primarily in the fidelity with which the plant is modeled and the accuracy of the identified model parameters. Hence, classical model-based control techniques seem to be neither optimal for hybrid MAVs nor easily transposable for a new platform. Gain scheduling methods employing different control algorithms with both linear [10] and nonlinear approaches [11], have been developed to stabilize hybrid MAVs at different pitch angle orientations within the transitioning flight. Gain scheduling techniques allow easy understanding and simple implementation of the control gains that cover the entire flight envelope of hybrid MAVs. However, the principal disadvantage of this control method, found in the literature [12], is the expensive computational cost for operations in real time. In the same way, an attitude controller based on optimal control algorithms was proposed by [13], different control solutions for a set of attitude errors were precomputed and stored in a lookup table. According to the current flight conditions and for each autopilot system update, the desired control informations are obtained by reading the predefined values from the table. Experimental flights proven that this control approach enable the hybrid MAV to recover from a significant range of attitude errors. Further analysis is needed to determine if this proposed control strategy can be effective and easily adaptable for different hybrid MAVs. Adaptive control techniques which account for uncertainties present in the hybrid MAV model were developed by [14] [15]. However, instability problems with adaptive control methods can still exist with regard to unmodeled dynamics or inaccurate models used in the adaptation criterion of controller's gains. Different research topics applying nonlinear control techniques on hybrid MAVs, such as backstepping [16], NDI [17] and INDI [18], appears to be positively researched in the literature. The INDI approach, which is a control that depends less on the model, was experimentally flight tested providing excellent performance against wind disturbances. This controller requires the identification of the system actuator behaviour in order to estimate its control effectiveness. As the actuators effectiveness vary according to the flight phase, e.g hovering or forward flight, a gain scheduling method was implemented to fit the actuator effectiveness under the respective flight domain. Some theoretical research analyzed the performance of nonlinear feedback control on axisymmetric aerial vehicles [19] proposing an extended control solution to a larger set of generic aerodynamic models [20] which could include hybrid MAVs. Additionally, a variety of nonlinear control strategies based on Lyapunov's stability concepts have been designed to hybrid MAVs [4] [21].

B. Links with Model-Free Control algorithm

Although most of the controls described in the literature, are designed according to a modelling process, we can mention some particular techniques where the controller does not rely on modelling. For instance, the model-free control approach proposed by [22] that have been successfully used in different concrete case-studies varying from wastewater denitrification [23], nanopositioning of piezoelectric systems [24] up to inflammation resolution in biomedical applications [25], see also its references for additional case-study examples and supplementary information. Some research works based on model-free control techniques has been led to patents, such as [26] [27]. In the aerospace field, this control approach has been little applied [28] [29] and, except for our previous work, it has never been applied on hybrid MAVs which is an additional motivation for the development of our research project. The advantage of the control methodology proposed in this paper is the capability to estimate the hybrid MAV dynamics, without a prior knowledge of its parameters, only from its output and input-control signal measurements. Thus, any disturbance that may affect the flight performance are measured and the MFC algorithms are able to estimate and counteract the undesirable dynamics in order to continuously stabilize the hybrid MAV for arbitrary attitude orientations.

II. Related Work

Hybrid MAVs have now reached a level of maturity such that the problem of improving their autonomous flight capabilities is now becoming a major concern. While the different flight aptitudes of hybrid MAVs enlarge their application range, autopilot systems must ensure the stability and the tracking trajectories of all flight domains which results in a higher degree of challenge and complexity for the guidance, navigation, and control community. Often, the control community considers the hybrid MAV model as a parameter-varying system, e.g. the change of aerodynamic coefficients according to the hybrid MAV attitude and the environmental wind conditions. Consequently, design a control technique for autopilot systems that does not rely on prior knowledge of the hybrid MAV model becomes an intuitive, innovative and, from the point of view of the authors, an appropriate control methodology. Therefore, the development of a such controller that estimates the hybrid MAV dynamics and counteracts it, in real time, can be easily adaptable and implemented for different hybrid MAVs. The reviewed control approaches for hybrid MAVs draw attention to the following points :

- Control systems are usually designed from a linearized model of the hybrid MAV behaviour. Nonlinear dynamics that include aerodynamic effects, such as propeller-wing interaction and stall phenomena, are not correctly represented in the linearized model around equilibrium points of the hybrid MAV.
- The entire flight envelope of hybrid MAVs, in terms of control design, is usually addressed by considering two different flight phases: one for hovering and one for forward flight. After the control design of each flight phase tackling their respective dynamics, the transitioning phase stability is assured by gain scheduling techniques or by switching between these two control designs.
- Model-based control approaches require an identification of aerodynamic forces and moments acting in the system in order to properly design the controller. This identification, especially for high incidence angles, remains a difficult, expensive and time consuming process.

This work focuses on the development of a new control architecture for hybrid MAVs composed of model-free control algorithms. We propose a control strategy that ensures the stability of the system without switching or gain scheduling methods contributing to the development of a unified control architecture. The present work covers different steps of flight dynamics field including control design, simulation flight analysis, algorithm implementation up to experimental flight tests. In terms of flight simulation, a good understanding of aerodynamic forces and moments that act in the system is required in order to define a realistic hybrid MAV flight simulator. Unfortunately, accurate and realistic hybrid MAV model remains a very complex task without certain simplifications. Thus, in the following section, we present a simplified tail sitter MAV model with its aerodynamic assumptions. The obtained tail sitter MAV model is used to establish a flight simulator in order to test the proposed control approach before of its implementation in real flight experiments. However, we emphasize that the tail sitter MAV dynamics are unknown to the control and they are not used to design the controller.

III. Simplified Tail Sitter MAV Model

We present an analytic continuous singularity-free formulation of aerodynamic forces $\boldsymbol{F_{a_b}} \in \mathbb{R}^3$ and moments $\boldsymbol{M_{a_b}} \in \mathbb{R}^3$ acting in a wing over a complete 360° angle of attack, based on previous work proposed by [30]. The wing with a surface S, is immersed in an incompressible and inviscid airflow with air density ρ. The free-stream velocity is composed by the linear element $\boldsymbol{v_\infty} \in \mathbb{R}^3$ and the angular component defined by $\boldsymbol{\omega_\infty} \in \mathbb{R}^3$ which, in the absence of wind, is equal to the hybrid MAV angular velocity $\boldsymbol{\omega_b} \in \mathbb{R}^3$. This formulation of aerodynamic forces and moments is given by :

$$\begin{pmatrix} \boldsymbol{F_{a_b}} \\ \boldsymbol{M_{a_b}} \end{pmatrix} = -\frac{1}{2}\rho S \eta C \Phi(\boldsymbol{\eta_b}) C \boldsymbol{\eta_b} \tag{1}$$

where

$$\eta = \sqrt{v_\infty^2 + \mu\, c^2 \omega_\infty^2}, \quad \text{with} \quad \mu \in \mathbb{R} > 0 \tag{2}$$

and

$$\boldsymbol{\eta_b} = \begin{pmatrix} \boldsymbol{v}_\infty \\ \boldsymbol{\omega}_\infty \end{pmatrix} \tag{3}$$

The vector $\boldsymbol{\eta_b}$ describes the linear and angular free-stream velocities in the body coordinate frame. The matrix C denotes the reference wing parameters in an extended representation,

$$C = \begin{pmatrix} I_{3\times3} & 0_{3\times3} \\ 0_{3\times3} & \begin{bmatrix} \mathrm{b} & 0 & 0 \\ 0 & \mathrm{c} & 0 \\ 0 & 0 & \mathrm{b} \end{bmatrix} \end{pmatrix} \tag{4}$$

where b and c are, respectively, the wingspan and the mean chord. Finally, the matrix $\Phi \in \mathbb{R}^{6\times6}$, which is subdivided into four matrices $\Phi^{(\cdot)} \in \mathbb{R}^{3\times3}$, shows the interaction between aerodynamic forces and moments with linear and angular free-stream velocities :

$$\Phi = \begin{pmatrix} \Phi^{(fv)} & \Phi^{(fw)} \\ \Phi^{(mv)} & \Phi^{(mw)} \end{pmatrix} \tag{5}$$

The Φ parameters are deduced from thin airfoil theory, we refer the interested reader to [30] for further information. Nonetheless, we mention that,

$$\Phi_0^{(fv)} = \begin{pmatrix} C_{d0} & 0 & 0 \\ 0 & C_{y0} & 0 \\ 0 & 0 & 2\pi + C_{d0} \end{pmatrix} \tag{6}$$

$$\Phi^{(f\omega)} = \begin{pmatrix} 0 & 0 & 0 \\ 0 & 0 & b^{-1}\Delta r C_{y0} \\ 0 & -c^{-1}\Delta r(2\pi + C_{d0}) & 0 \end{pmatrix} \tag{7}$$

$$\Phi_0^{(mv)} = \begin{pmatrix} 0 & 0 & 0 \\ 0 & 0 & -c^{-1}\Delta r(2\pi + C_{d0}) \\ 0 & b^{-1}\Delta r C_{y0} & 0 \end{pmatrix} \tag{8}$$

$$\Phi^{(m\omega)} = \frac{1}{2}\begin{pmatrix} C_{l_p} & C_{l_q} & C_{l_r} \\ C_{m_p} & C_{m_q} & C_{m_r} \\ C_{n_p} & C_{n_q} & C_{n_r} \end{pmatrix} \tag{9}$$

with C_{d0} the minimal drag coefficient and C_{y0} the minimal side force coefficient. The parameter Δr represents the distance between the center of gravity location and the aerodynamic center (neutral point). The negative values of Δr, according to the defined coordinate system, imply a positive static margin of the hybrid MAV. Finally, C_l, C_m and C_n are the aerodynamic moment coefficients which depend on the angular hybrid MAV velocities (p, q, r). The lift curve slope corresponding to 2π, in (6), (7) and (8), was deduced from the thin airfoil theory in 2D. In this work, we evaluate the lift curve slope in 3D considering the wing aspect ratio (AR). According to Diederich's formula, we consider :

$$\Phi_0^{(fv)}(:,3) = \begin{pmatrix} 0 \\ 0 \\ \frac{\pi AR}{1+\sqrt{1+(\frac{AR}{2})^2}} + C_{d0} \end{pmatrix} \tag{10}$$

$$\Phi^{(f\omega)}(:,2) = \begin{pmatrix} 0 \\ 0 \\ -c^{-1}\Delta r\Big(\frac{\pi AR}{1+\sqrt{1+(\frac{AR}{2})^2}} + C_{d0}\Big) \end{pmatrix} \tag{11}$$

$$\Phi_0^{(mv)}(:,3) = \begin{pmatrix} 0 \\ -c^{-1}\Delta r\Big(\frac{\pi AR}{1+\sqrt{1+(\frac{AR}{2})^2}} + C_{d0}\Big) \\ 0 \end{pmatrix} \tag{12}$$

where

$$AR = \frac{b^2}{S} \tag{13}$$

Finally, the flap deflections are modeled as varying cambered airfoils and the aerodynamic forces and moments created by these deflections are approximated by the following equations :

$$\Phi^{(fv)}(\delta_i) = \Phi_0^{(fv)}(I - [\boldsymbol{\xi_f}]_\times \delta_i) \tag{14}$$

$$\Phi^{(mv)}(\delta_i) = \Phi_0^{(mv)}(I - [\boldsymbol{\xi_m}]_\times \delta_i) \tag{15}$$

the flap deflection effectiveness is represented by two skew-symmetric matrices, $[\boldsymbol{\xi_f}]_\times$ for the force effectiveness and $[\boldsymbol{\xi_m}]_\times$ for the moment effectiveness, given by :

$$[\boldsymbol{\xi_f}]_\times = \begin{bmatrix} 0 & -\xi_f & \xi_f \\ \xi_f & 0 & -\xi_f \\ -\xi_f & \xi_f & 0 \end{bmatrix}$$

$$[\boldsymbol{\xi_m}]_\times = \begin{bmatrix} 0 & -\xi_m & \xi_m \\ \xi_m & 0 & -\xi_m \\ -\xi_m & \xi_m & 0 \end{bmatrix}$$

A. Equations of motion

The tail sitter MAV model is divided into four rigid bodies (two propellers and one fuselage composed by two wings) with constant mass (m), represented by ten states $\boldsymbol{x} = (\boldsymbol{v_b}, \boldsymbol{\omega_b}, \boldsymbol{q})$, where $\boldsymbol{v_b} \in \mathbb{R}^3$ is the vehicle's linear velocity, $\boldsymbol{\omega_b} \in \mathbb{R}^3$ is the vehicle's angular velocity equals to $[p\ q\ r]^T$ both expressed in the body coordinate frame and $\boldsymbol{q} \in \mathbb{R}^4$ is the quaternion formulation. The system is controlled via four control-inputs, $\boldsymbol{u} = (\omega_l, \omega_r, \delta_l, \delta_r)$, respectively, the left and right propeller rotation speeds and the left and right flap deflections, which are represented in the Fig. 2. In order to compute the forces and moments caused by the wing-propeller interaction, we define two segments. Each segment is composed by one wing j and by one propeller k. Thus, the sum of aerodynamic forces acting on the wing j with the thrust $\boldsymbol{T}_k$ generated by the propeller rotation ω_k and the total moment described in the body coordinate frame, are given by :

$$\boldsymbol{F_b} = \sum_{j,k=1}^{2} (\boldsymbol{F_{a_{b_j}}} + \boldsymbol{T}_k) \tag{16}$$

$$\boldsymbol{M_b} = \sum_{j,k=1}^{2} (\boldsymbol{M_{a_{b_j}}} + \boldsymbol{\tau_{b_k}} + \boldsymbol{p_p} \times \boldsymbol{T}_k + \boldsymbol{p_a} \times \boldsymbol{F_{a_{b_j}}}) \tag{17}$$

The vector $\boldsymbol{p_p} = [p_{p_x}\ p_{p_y}\ p_{p_z}]^T$ defines the distance between the propeller k with the hybrid MAV center of mass. Both propellers are positioned symmetrically with respect to the hybrid MAV center of mass. The distance between the

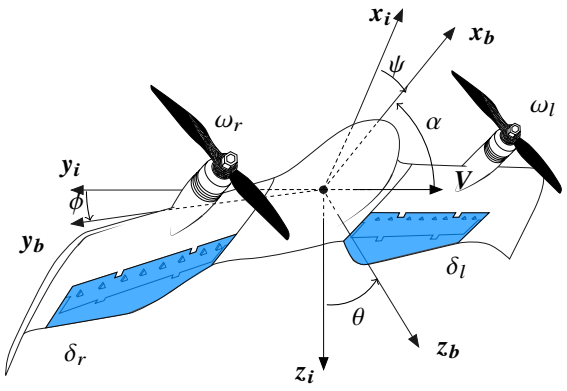

Fig. 2 Illustration of the used coordinate frames, angles and actuators. The inertial coordinate frame is represented by $\mathcal{R}_i = \{\boldsymbol{x_i}, \boldsymbol{y_i}, \boldsymbol{z_i}\}$ and the body coordinate frame by $\mathcal{R}_b = \{\boldsymbol{x_b}, \boldsymbol{y_b}, \boldsymbol{z_b}\}$.

aerodynamic center and the center of mass is represented by the vector $\boldsymbol{p_a} = [p_{a_x}\ p_{a_y}\ p_{a_z}]^T$. The internal torque of the propeller $\boldsymbol{\tau_{b_k}}$ that is a function of the vehicle's angular velocity $(p\ q\ r)$, and the thrust force $\boldsymbol{T}_k$, are defined by :

$$\boldsymbol{T}_k = k_f \omega_k^2\, \boldsymbol{x_b}, \qquad k_f \in \mathbb{R} > 0 \tag{18}$$

$$\boldsymbol{\tau_{b_k}} = \boldsymbol{N_{b_k}} - J_p\,(p + \omega_j) \begin{pmatrix} 0 \\ r \\ -q \end{pmatrix} \tag{19}$$

where

$$\boldsymbol{N_{b_k}} = -\text{sign}(\omega_k) k_m \omega_k^2\, \boldsymbol{x_b}, \qquad k_m \in \mathbb{R} > 0 \tag{20}$$

with k_f and k_m the propeller force and moment coefficients and $\boldsymbol{N_{b_k}}$ the propeller moment. Equation (19) describes the gyroscopic interaction between the propellers and the fuselage with J_p equals to the propeller inertia. The vehicle's equations of motion are given by (21).

$$\begin{cases} m\,\dot{\boldsymbol{v}} & = R^T \boldsymbol{F_b}(\boldsymbol{x}, \boldsymbol{u}, \boldsymbol{W}) + m\boldsymbol{g} \\ J\,\dot{\boldsymbol{\omega_b}} & = \boldsymbol{M_b}(\boldsymbol{x}, \boldsymbol{u}, \boldsymbol{W}) - [\boldsymbol{\omega_b}]_\times J \boldsymbol{\omega_b} \\ \dot{\boldsymbol{q}} & = \frac{1}{2}\boldsymbol{q} * \boldsymbol{\omega_b} \\ \dot{\boldsymbol{p}} & = \boldsymbol{v} \end{cases} \tag{21}$$

The gravitational acceleration vector is equals to $\boldsymbol{g} = g\boldsymbol{z_i}$ and $\boldsymbol{W} \in \mathbb{R}^3$ is the wind disturbance vector. The rotation matrix R, namely the Direction Cosines Matrix (DCM), represents the MAV rotation in three dimensions as a mathematical formulation. We assume that the hybrid MAV inertia matrix J is diagonal and it equals to $J = \text{diag}\,[J_{xx}\ J_{yy}\ J_{zz}]$. The position vector in the inertial coordinate frame is represented by $\boldsymbol{p} = [x\ y\ z]^T$. The highly maneuverable nature of the vehicle calls for a global numerically stable formulation of attitude and justifies the use of quaternions. The symbol $*$ in the previous equation corresponds to the quaternion product.

IV. Model-Free Control

The following section outlines briefly the main features of model-free control approach and some previous research-works dealing with on-line dynamic state estimation. These research-works have been applied in different areas of the science including aerospace systems. However, we present for the first time the development of a such controller for hybrid MAVs.

A. Principles

As introduced by [22], an unknown finite-dimensional system with a single control-input (u) and a single output (y) can be described by the following input/output relation in a differential equation formulation :

$$\mathbb{E}(y, \dot{y}, \ldots, y^{(a)}, u, \dot{u}, \ldots, u^{(b)}) = 0 \tag{22}$$

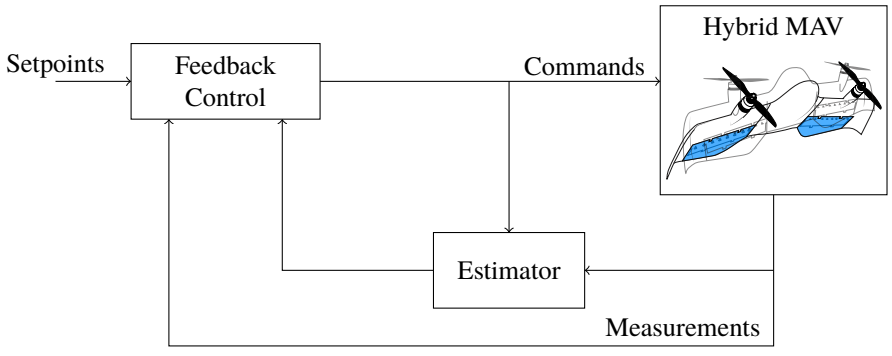

Fig. 3 Overall Model-Free Control schema for hybrid MAVs.

where $\mathbb{E}$ is a polynomial function with real unknown coefficients. We can also describe

$$y^{v} = \mathbb{E}(t, y, \dot{y}, \ldots, y^{(v-1)}, y^{(v+1)}, \ldots, y^{(a)}, u, \dot{u}, \ldots, u^{(b)}) \tag{23}$$

with $0 < v \leq a$ and $\frac{\delta \mathbb{E}}{\delta y^{v}} \neq 0$. This unknown dynamic can be approximated by a purely numerical equation, the so-called *Ultra-Local Model* :

$$y_m^{(v)} = F_y + \lambda \cdot u \tag{24}$$

In (24), v is the order derivative of y_m, $\lambda \in \mathbb{R}$ is a non-physical constant parameter. Moreover, the exploitation of this numerical model requires the knowledge of F_y. This quantity represents the real dynamics of the model as well as the different disturbances which could damage the performance of the output-system. Thus, an accurate estimation of F, defined as $\hat{F}$, is crucial and plays an import role in the control performance. Different practical experiments proved that a first order *Ultra-Local Model* ($v = 1$) is enough to stabilize with precision an unknown dynamic. In this work, we propose to develop a second-order *Ultra-Local Model* ($v = 2$) due to viscous friction and actuator dynamics that could add an extra order to the system. Assuming that we do not have any information about an arbitrary second order dynamic, its estimation can be computed directly by the following methodology, see algorithm (1).

Algorithm 1 Computing the estimator $\hat{F}$

1: **procedure**
2: $v \leftarrow$ Define estimator order
3: **step 1:** Write the *Ultra-Local Model*
4: **step 2:** Calculate the *Laplace transforms*
5: **step 3:** Derive step 2 v times with respect to s
6: **step 4:** Multiply the step 3 by $s^{-(v+1)}$
7: **step 5:** Calculate the *Inverse Laplace transforms*
8: **end procedure**;

In a mathematical formulation, we obtain :

$$\ddot{y}_m = F_y + \lambda \cdot u \tag{25}$$

The first step is to apply the *Lapace Transform* in (25). Referring to elementary operational calculus we transform (25) to (26) :

$$s^2 Y_m(s) - s y_m(0) - \dot{y}_m(0) = \frac{F_y}{s} + \lambda U(s) \tag{26}$$

Where $Y_m(s)$ and $U(s)$ correspond to the *Laplace transforms* of y_m and u. By differentiating twice the previous equation we are able to rid the initial conditions $y_m(0)$ and $\dot{y}_m(0)$:

$$2Y_m(s) + 4s\frac{dY_m(s)}{ds} + s^2\frac{d^2Y_m(s)}{ds^2} = \frac{2F_y}{s^3} + \lambda\frac{d^2U(s)}{ds^2} \tag{27}$$

However, the variable s in the time domain corresponds to the derivation with respect to time that is sensitive to noise corruptions and can amplify the noise measurement. Therefore, in order to reduce both noise and numerical computation errors on the output estimation, we replace the derivative terms by integrators ($\frac{1}{s}$) who have robust properties with respect to noise. Thus, multiplying both sides of (27) by s^{-3}, we obtain :

$$\frac{2Y_m(s)}{s^3} + \frac{4}{s^2}\frac{dY_m(s)}{ds} + \frac{1}{s}\frac{d^2Y_m(s)}{ds^2} = \frac{2F_y}{s^6} + \frac{\lambda}{s^3}\frac{d^2U(s)}{ds^2} \tag{28}$$

Equation (28) can be transferred back to the time domain employing elementary calculus and *Cauchy's formula* to reduce multiple integrals in a simple one :

$$\hat{F_y} = \frac{5!}{2T^5}\int_{t-T}^{t}[(T-\sigma)^2 - 4\sigma(T-\sigma) + \sigma^2]y_m(\sigma) - [\frac{\lambda}{2}\sigma^2(T-\sigma)^2 u(\sigma)]d\sigma \tag{29}$$

From measurements of the corrupted signal y_m and u obtained in the last T seconds, the unmodeled dynamic of y and the disturbances are estimated by $\hat{F_y}$ which is updated for each interval of integration $[t-T, t]$. This interval corresponds

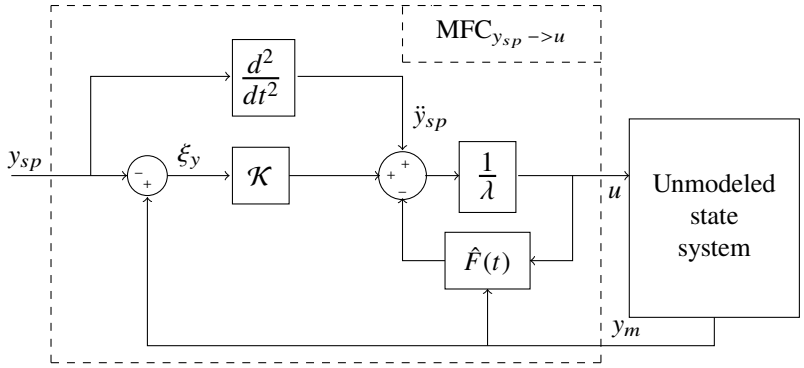

Fig. 4 Detailled model-free control schema.

to the window width of a receding horizon strategy which results in a trade-off. The idea is to choose the window width small so as to calculate the estimation within an acceptable short delay but large enough in order to preserve the low-pass filter properties for suppressing measurement noise on y_m. Based on such estimator, it is possible to design a robust controller that estimates the system dynamic on-line by a piecewise constant function $\hat{F}_y$ periodically updated for each measure of y_m and u. The detailed form of the MFC schema presented in Fig. 4 allows us to define the closed-loop control such as :

$$u = \underbrace{-\frac{\hat{F}_y}{\lambda}}_{\text{Nonlinear Cancellation}} + \underbrace{\frac{y_{sp}^{(2)} + \mathcal{K}(\xi)}{\lambda}}_{\text{Closed loop tracking}} \tag{30}$$

where the quantity $\xi = y_m - y_{sp}$ is the tracking error and $\mathcal{K}(\xi)$ is a closed loop feedback controller, usually defined as a proportional, proportional-derivative or even so as proportional-integral-derivative gain. In this paper, we define the closed loop feedback controller as a proportional K_p and derivative gain K_d. We recognize in (30) the typical mathematical expression of a nominal control in the flatness-based in which the non-linear terms $\hat{F}_y$ is added with a closed loop tracking of a reference trajectory $t \rightarrow y_{sp}(t)$. The error dynamic can be deduced from the combination of (30) with (25) :

$$\ddot{\xi}_y = \ddot{y}_m - \ddot{y}_{sp} = \overbrace{F_y - \hat{F}_y}^{\xi_{F_y} \approx 0} + K_p\, \xi_y + K_d\, \dot{\xi}_y \tag{31}$$

$$\ddot{\xi}_y - K_d\, \dot{\xi}_y - K_p\, \xi_y = 0 \tag{32}$$

Note that, if the error (ξ_{F_y}) between the estimator and the true dynamic, is approximately zero during $[t - T, t]$, a simple proportional-derivative controller will be enough to ensure the error convergence to zero if $K_p < 0$ and $K_d < 0$. Whereas, an integration effect is implicitly involved in the model-free control algorithm.

B. Discretized MFC equations

Expressing (25) in discrete-time domain, with k the index of the current sampling time T_s, we obtain

$$\frac{y_m(kT_s) - 2y_m(kT_s - T_s) + y_m(kT_s - 2T_s)}{T_s^2} = F(kT_s) + \lambda u(kT_s) \tag{33}$$

where the left-hand side (LHS) of (33), represents the discrete second order derivative of y_m. The discretized plant model $F(kT_s)$ represents not only the dynamic of $y_m[kT_s]$ but also the different disturbances which could damage the output-system. $u(kT_s)$ is the input-control signal, λ a constant parameter that allows us to set the same magnitude between the LHS of (33) and $\lambda u(kT_s)$. The dynamic of a SISO system is approximated by a linear model, called *Ultra-Local Model*, that is valid around a given operating point, i.e. $[kT_s, kT_s - T\,T_s]$. Different operating points may lead to several different linear models that are continuously estimated by $\hat{F}(kT_s)$. The discretized closed loop tracking is achieved by using a proportional and derivative gain, yielding the control-input $u(kT_s)$ in (34).

$$u(kT_s) = \underbrace{-\frac{\hat{F}(kT_s)}{\lambda}}_{\text{Nonlinear Cancellation}} + \underbrace{\frac{y_d^{(v)}(kT_s) + K_p\, \xi(kT_s) + K_d\, \dot{\xi}(kT_s)}{\lambda}}_{\text{Closed loop tracking}} \tag{34}$$

where $y_d^{(v)}(kT_s)$ denotes the v-th order derivative of y_d. The tracking error $\xi(kT_s)$ and the derivative of the tracking error $\dot{\xi}(kT_s)$, are defined respectively as

$$\xi(kT_s) = y_m(kT_s) - y_d(kT_s) \tag{35}$$

$$\dot{\xi}(kT_s) = \dot{y}_m(kT_s) - \dot{y}_d(kT_s) \tag{36}$$

Remark : The derivative of the tracking error can be measured directly in the system or computed with simple finite difference formulas such as backward finite difference. In this case, the derivative of the tracking error is :

$$\dot{\xi}(kT_s) = \frac{\xi(kT_s) - \xi(kT_s - T_s)}{T_s} \tag{37}$$

Substituting the control-input $u(kT_s)$ from (34) in (33), we obtain the following expression :

$$\begin{aligned} \underbrace{y_m(kT_s) - 2\,y_m(kT_s - T_s) + y_m(kT_s - 2T_s)}_{\text{Numerical second-order derivative of } y_m} &= \overbrace{F(kT_s) - \hat{F}(kT_s)}^{\xi_F \approx 0} \\ &+ \underbrace{y_d(kT_s) - 2\,y_d(kT_s - T_s) + y_d(kT_s - 2T_s)}_{\text{Numerical second-order derivative of } y_d} \\ &+ K_p\,\xi(kT_s) + K_d\,\dot{\xi}(kT_s) \end{aligned} \tag{38}$$

If $\xi_F \approx 0$, then the effect of disturbances is negligible on the error dynamic.

$$\begin{aligned} \ddot{\xi}(kT_s) = &\frac{y_m(kT_s) - 2y_m(kT_s - T_s) + y_m(kT_s - 2T_s)}{T_s^2} \\ &- \frac{y_d(kT_s) + 2y_d(kT_s - T_s) - y_d(kT_s - 2T_s)}{T_s^2} \end{aligned} \tag{39}$$

So, (40) shows that

$$\ddot{\xi}(kT_s) = K_p\xi(kT_s) + K_d\dot{\xi}(kT_s) \tag{40}$$

We can see that the system can be guaranteed to be stable if K_p and K_d are negatives and the control law (34) can be shown to be stable resulting in $\xi(kT_s) \to 0$ as $kT_S \to \infty$. The algorithm (2) describes the main steps of the MFC.

Algorithm 2 Model-free Control algorithm

procedure INITIALIZATION
    Define sampling time $\to T_s$
    Initial conditions $\to \boldsymbol{x_0}, \boldsymbol{u_0}$
    Define MFC parameters $\to \lambda, T, K_p$ and K_d
end procedure;
procedure MFC COMMAND
Control loop:
    Define the desired trajectory $\to y_d[kT_s]$
    Read output measurement $\to y_m[kT_s]$
    Read control value from the last sampling period $\to u[kT_s - T_s]$
    Compute the discretized estimator from equation $\to \hat{F}[kT_s]$
    Compute error $\to \xi[kT_s]$
    Compute closed-looping tracking $\to \mathcal{K}(\xi)$
    Compute new command from equation (34) $\to u[kT_s]$
goto *Control loop*
end procedure;

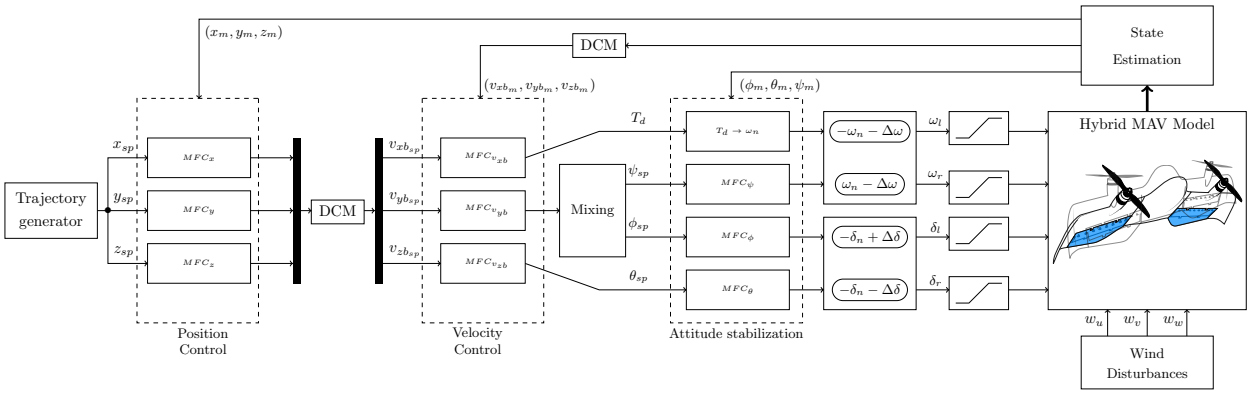

Fig. 5 Cascaded MFC architecture designed for hybrid MAVs. Velocity control block receives desired ground velocities and computes references for attitude stabilization control loop. Based on these desired values, propeller speeds (ω_l, ω_r) and flap deflections (δ_l, δ_r) are defined.

C. Proposed MFC architecture

Figure 5 shows the main ideas of our control architecture. The block *Trajectory generator* is composed of a state flow algorithm that defines constantly the desired positions (x_{sp}, y_{sp}, z_{sp}) in the inertial coordinate system. These references are taken into account by the *Position control* block and are compared with the respective measures (x_m, y_m, z_m) creating three errors that are minimized by the MFC algorithms in the *Position control* block. These three MFC algorithms in charge of the position tracking, also compute the desired velocity in their respective axes. These references values which are defined in the inertial coordinate frame are transformed to the body coordinate frame as well as the velocities measurements. Thus, the velocity control MFC$_{v_{xb}}$ computes the required thrust T_d to reach this desired velocity along $\boldsymbol{x_b}$, the block MFC$_{v_{zb}}$ assures the velocity control along $\boldsymbol{z_b}$ and determine the necessary pitch angle θ_{sp} to reach this desired velocity $v_{zb_{sp}}$. Both blocks control their respective velocities and inform the desired thrust and pitch angle for the entire flight envelope, i.e. hover, transition and forward flight. However, the velocity control along $\boldsymbol{y_b}$ is designed depending on the current hybrid MAV flight phase. Therefore, in hover flight, the block MFC$_{v_{yb}}$ set the desired yaw angle ψ_{sp} and the block MFC$_{\psi}$ actuates in the system by a differential-thrust command creating a moment around $\boldsymbol{z_b}$ in order to reach the desired velocity along $\boldsymbol{y_b}$. In forward flight, this lateral velocity is reached from roll rotations around $\boldsymbol{x_b}$. These rotations orient the lift force and the hybrid MAV can perform left-right turns with, respectively, negative and positive roll angles ϕ. The propeller speeds (ω_l, ω_r) are defined by the sum of nominal propeller rotation ω_n with a differential propeller speed Δ_ω which is in charge of the yaw control. The negative sign of ω_n for the left-propeller ω_l is due to the counter-rotation sense. And the flap-deflections (δ_l, δ_r), which are in convention negative for pitch-up, are composed by the sum of symmetrical flap deflection δ_n with anti-symmetrical flap deflections Δ_δ that are respectively the control-input for the pitch angle θ and for the roll angle ϕ. We compute the control-output of each block according to the algorithm described beforehand, algorithm (2).

V. DarkO Tail Sitter MAV

Throughout the whole study, we have used the DarkO vehicle which is a tail-sitter configuration consisting of two motors, positioned in front of the wing, and two exceptionally large double-flapped control surfaces, see Fig. 6. We briefly present its manufacturing process and the characteristics of motors, propellers, servos, and battery that were used during the experimental flight tests.

A. Setup and specifications

Mission definition of DarkO has been mainly oriented for forward flight with the capability of taking off and landing vertically. The frame completely manufactured by 3-D printing method using Onyx material. Figure 7 shows the printed pieces that is assembled in order to build the whole frame. The shell structure for the wing and the fuselage halves are manufactured as $0.7mm$ thick skins, and the spar is manufactured with the addition of unidirectional concentric carbon fibres embedded into Onyx material. This method ensures to have a sufficiently rigid airframe that supports

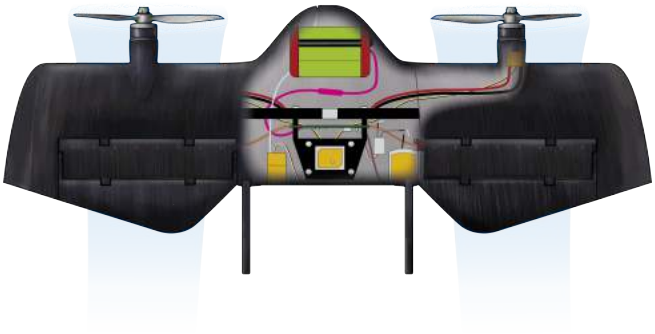

Mass	0.492 Kg
Wingspan	0.55 m
Mean Chord	0.13 m
Propellers	2-blades Bullnose 5x4.5
Motors	T-Motor Brushless F30 2800KV
Servos	MKS DS65K 0.2s/60°
Battery	3 cells 12V 3500 mAh

Fig. 6 General DarkO tail sitter MAV specifications.

aerodynamic forces and yet also flexible enough to absorb harsh impacts during landing and test flights. The different physical and geometric parameters of the DarkO MAV, are described in the Table 1. Inertia coefficients were estimated by using the classical pendulum method and the aerodynamic coefficients calculated from the open-source program XFOIL [31]. These different parameters were used in the simplified hybrid MAV model, described in the following section, in order to develop, analyze and validate the proposed control architecture, as realistic as possible, in simulation before the experimental flights.

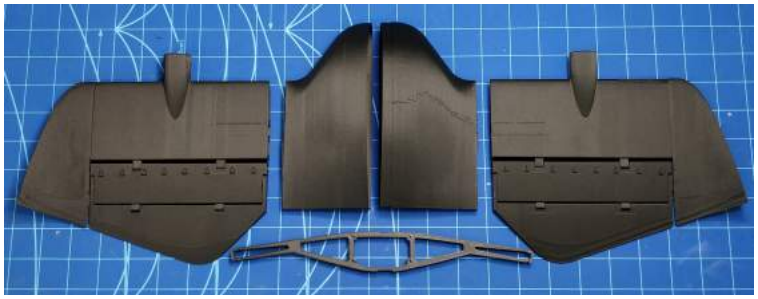

Fig. 7 Printed parts of DarkO out of Onyx material.

B. Actuators and attitude dynamics

The attitude dynamic is controlled according to the actuation principle described in the Fig. 8, 9, and 10. Hybrid MAVs are characterized as nonlinear systems with high coupled dynamics. In fact, pitch and roll angles are controlled respectively by symmetric and asymmetric flap deflections who are dependents of the propeller slipstream. The differential thrust in order to control the yaw angle modifies the propeller slipstream impacting the control-effectiveness

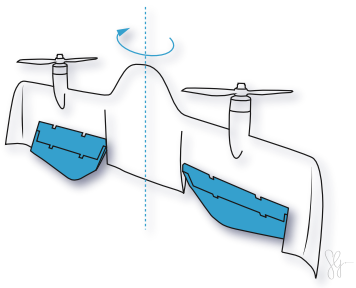

Fig. 8 Roll angle dynamic

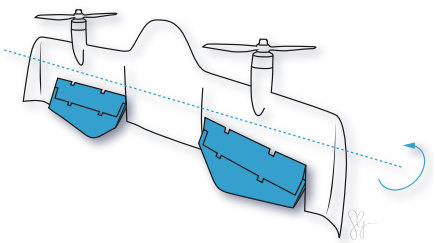

Fig. 9 Pitch angle dynamic

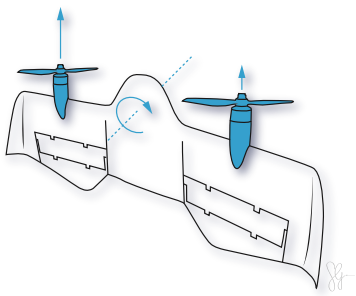

Fig. 10 Yaw angle dynamic

Table 1 DarkO MAV parameters used during flight simulations.

Parameters	Values	SI Units
Mass (m)	0.492	[Kg]
Mean Chord (c)	0.135	[m]
Wingspan (b)	0.55	[m]
Wing Area (S)	0.0743	[m^2]
J_{xx}	0.004 93	[Kg m^2]
J_{yy}	0.005 32	[Kg m^2]
J_{zz}	0.008 62	[Kg m^2]
J_p	5.1116×10^{-6}	[Kg m^2]
k_f	5.13×10^{-6}	[Kg m]
k_m	2.64×10^{-7}	[Kg m^2]
C_{d0}	0.133	No units
C_{y0}	0.145	No units
C_l	[0.47; 0.00; 0.00]	No units
C_m	[0.00; 0.54; 0.00]	No units
C_n	[0.00; 0.00; 0.52]	No units

of the flaps as well as the dynamic of both pitch and roll angles.

C. Control surface design

A particular feature that is required by the tail-sitter configuration is to generate excessive amount of pitching moment in order to transition mainly from forward flight phase to hovering flight phase. Therefore, DarkO frame's control surfaces have been designed as double-flap which has a passive mechanical constant ratio. Traditionally, multisection flaps have been designed for lift enhancement, however in our case the design objective is to generate as much positive pitching moment as possible without having a massive flow separation on the bottom surface of the airfoil.

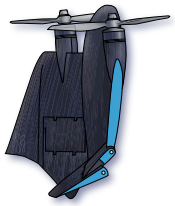

D. On-board avionics

The DarkO MAV is equipped with an *Apogee v1.00* board, presented in the Fig. 11, that contains a Cortex M4 168 MHZ processor to run the *Paparazzi* open-source autopilot system, which includes algorithms for state estimation, control laws, servo and motor drivers, software for communication, etc. In addition, the *Apogee v1.00* board is equipped with a SD logger which allows us to record the flight data for flight post-processing analysis.

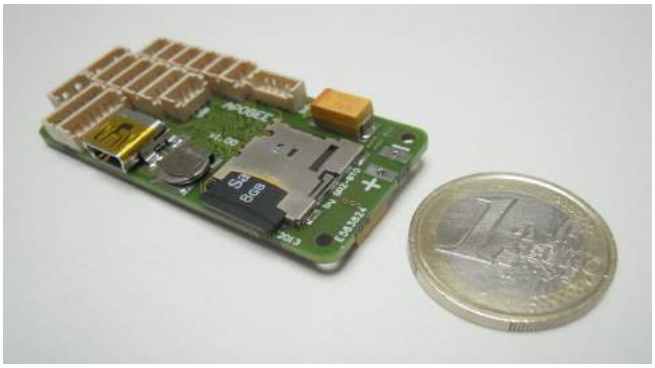

STM32F405RGT6 Cortex M4 168MHz processor
9(6) DOF integrated IMU MPU-9150(6050)
1 x Barometer/altimeter MPL3115A2
1 x MicroSD card slot
4 bit SDIO interface (high speed data logging)
6 x Servo PWM outputs
3 x UART, 2 x I2C bus, 1 x SPI bus
10.4 grams
53 mm x 25 mm

Fig. 11 Overview of *Apogee v1.00* autopilot from *Paparazzi Autopilot system*.

Inertial measurement units (IMUs) typically contain rate-gyroscopes and accelerometers on three axes, measuring angular velocities and linear accelerations respectively. By processing signals from these devices, with attitude and heading reference system (AHRS) and inertial navigation system (INS), it is possible to obtain the attitude orientations, velocities and positions of an air vehicle. The main features of each sensor device embedded in the *Apogee v1.00* board, is presented in the Table 2.

Table 2 *Apogee V1.00* embedded sensors

	Device	Noise	Bias
Accelerometer	MPU-9150	400 ($\mu g/\sqrt{Hz}$)	150 (mg)
Rate-Gyro	MPU-9150	0.005 ($^\circ/s/\sqrt{Hz}$)	20 ($^\circ/s$)
Magnetometer	MPU-9150	N/A	N/A
GNSS position	NEO-6M	σ = 2.5 (m)	0 (m)
GNSS velocity	NEO-6M	σ = 0.1 (m/s)	0 (m/s)

VI. Flight Simulations

A comprehensive set of flight simulations for hybrid MAV, discretized at 500 Hz, were performed from MATLAB/Simulink using the tail sitter MAV model described in the Section III that is controlled by the proposed MFC architecture, see Fig. 5. Our flight simulator is based on the DarkO hybrid MAV physical parameters including sensor measurements which were corrupted by gaussian white noises whose standard deviations can be found in [32]. An invariant observer [33] is used providing a smoother signal measurement of the MAV states, this operation adds delays in the closed loop and must be taken into account during the controller's synthesis. The MFC parameters, i.e. λ_i, T_i, Kp_i and Kd_i, were tuned for the entire flight envelope and are the same for all flight simulations. In particular, two different experiments were performed. First, we analyze the capabilities of the control architecture to recover the hybrid MAV from different initial conditions to a stable setpoint in hovering flight mode. In this flight simulation, only the velocity and the attitude stabilization blocks are activated. Then, we check the entire flight envelope of hybrid MAVs with the positioning tracking, velocity control and attitude stabilization as well.

A. Initial condition analysis in hovering flight

The initial conditions for pitch angle and for forward speed during the hovering flight (θ_{ic} and $V_{x_{ic}}$), follow a normal distribution law according to (29) and (30).

$$\theta_{ic} \sim \mathcal{N}\left(\frac{\pi}{2}, \left(\frac{\pi}{6}\right)^2\right). \tag{29}$$

$$V_{x_{ic}} \sim \mathcal{N}\left(0, \left(\frac{5}{3}\right)^2\right). \tag{30}$$

The stability boundary presented in the Fig. 12, was empirically defined by evaluating all recovery trajectories from initial conditions to the desired setpoint. The desired setpoint corresponds to a stationary flight in the vertical position, respectively, 0 m/s for the forward speed and 90° for the pitch angle. Basically, three classes of trajectories were distinguished during these simulations. The first one combines trajectories with initial pitching angles larger than 90° with positive initial conditions for forward speeds. Likewise, trajectories with initial pitching angles smaller than 90° and negative initial conditions for forward speeds are also included in this class. The peculiarity of these trajectories is that, both converge directly to the desired equilibrium setpoint with small oscillations in the response time. This can be explained by the fact that, for initial pitching angles larger than 90°, the thrust vector is already well-oriented and it can be increased in order to decelerate the initial positive forward speeds. This thrust vector is increased from increments of the propeller rotations, which improves the flap effectiveness creating a powerful pitch moment that can easily orientate the attitude of the hybrid MAV in the right direction, towards the attitude setpoint. The same reasoning can be done for initial pitching angles smaller than 90° with negative forward speeds. In this initial flight condition and orientation, the controller generates the thrust vector in order to increase the forward speed resulting in an effective pitch moment which also steer the hybrid MAV towards the setpoint. The second class of trajectories is composed by

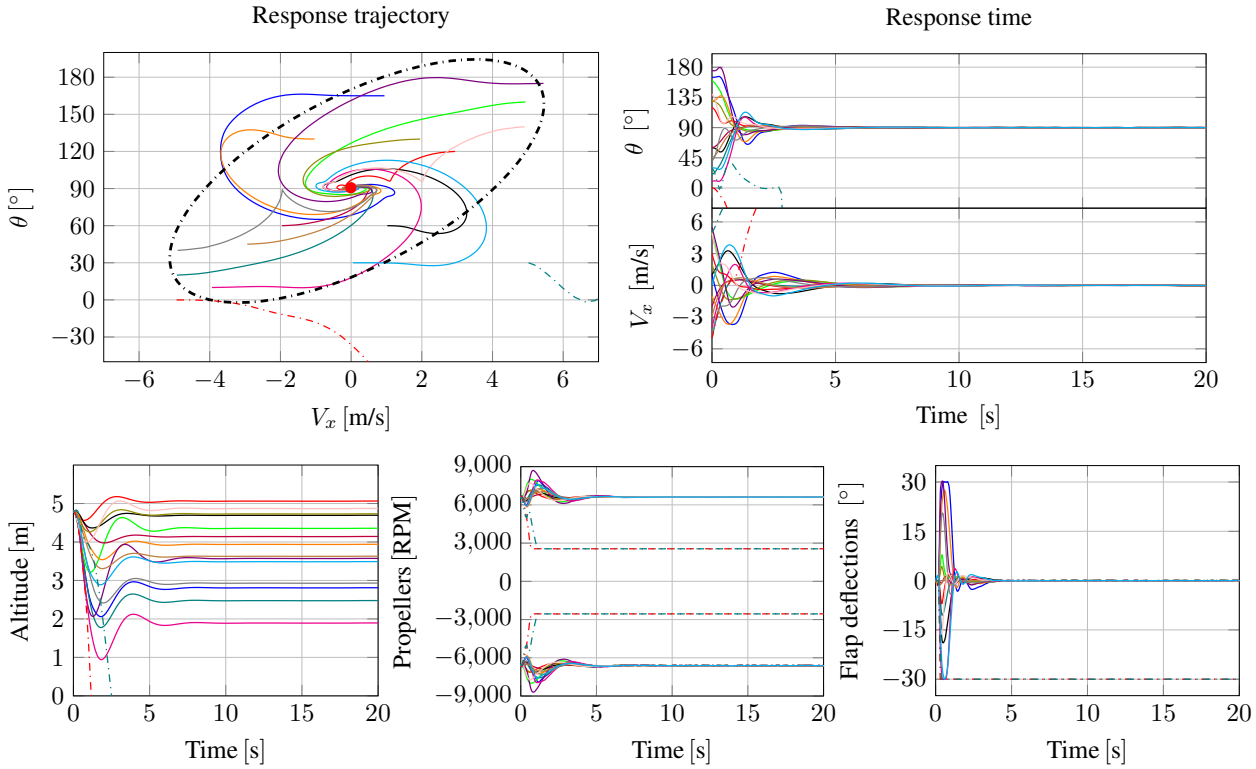

Fig. 12 Initial pitch angle and forward speed condition analysis during hovering flight phase without wind disturbances. Forward speed setpoint equals to 0 m/s, the MFC architecture computes the pitch angle setpoint equals to 90° in order to reach the stationary flight.

all initial pitching angles smaller than 90° with positive initial forward speeds and by all initial pitching angles larger than 90° with negative initial forward speeds. These trajectories diverge at the beginning of the simulation. The thrust vector, in these flight orientations, is unable to generate an opposing force to decelerate the initial forward speed to zero. The only force opposing to the movement is the drag force. By increasing the pitch angle, in this case the angle of attack, the hybrid MAV generates more drag and can reach the forward speed setpoint. For extreme cases, within the stability boundary, we can observe flap saturations which justify the shape of the concerned trajectories with overshoots or undershoots. By analyzing the altitude results, we can mention that the position control is not activated. However, we can observe that the altitude is stabilized at given values according to the velocity control block which cancels the vertical velocity component. The MFC can theoretically ensure a stable flight for all initial points inside the boundary, with more or less oscillations, according to the initial conditions. Otherwise, the hybrid MAV performs an unstable flight, as shown by the two particular initial points outside the stability boundary corresponding to the third class of trajectories in this simulation.

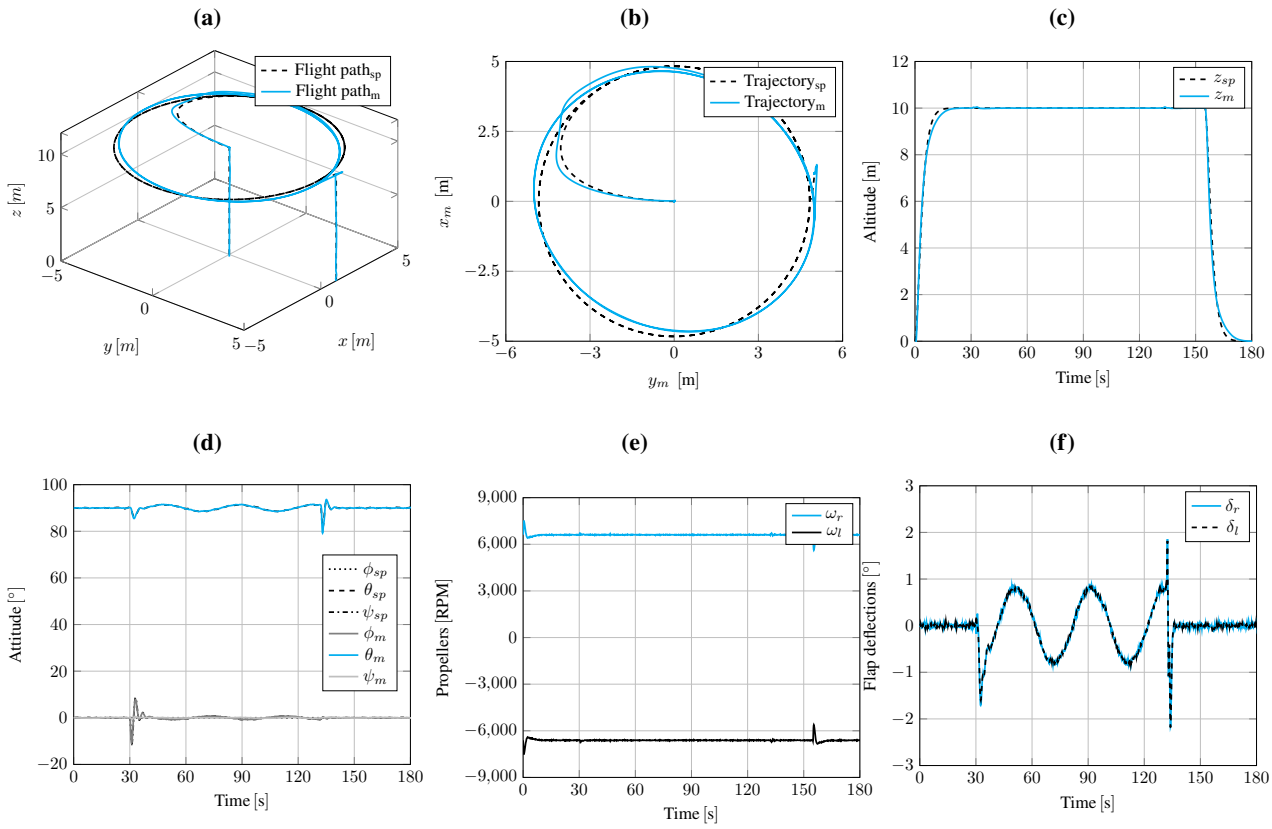

Fig. 13 Circular position tracking in hover flight mode. On the top, from left to right: the 3D flight path, North and East positions and altitude. On the bottom: attitude, propeller speeds and flap deflections.

B. Position tracking in hovering flight

In the second flight simulation, we impose a circular setpoint path in order to validate the interaction between all control blocks in the proposed control architecture. The following equations define the desired flight path,

$$x_{sp} = \begin{cases} 0, & t < 30s \\ x_c + r\,cos\left(\frac{2\pi}{40}t\right), & t \in [30;130]s \\ 1, & t > 130s \end{cases}$$

$$y_{sp} = \begin{cases} 0, & t < 30s \\ y_c + r\,sin\left(\frac{2\pi}{40}t\right), & t \in [30;130]s \\ 5, & t > 130s \end{cases}$$

$$z_{sp} = \begin{cases} 10, & t \in [0;155]s \\ 0, & t > 155s \end{cases}$$

where x_c and y_c correspond to the center of the circle and r is its radius. This maneuver requires the hybrid MAV to fly along a circular trajectory while constantly pointing its nose towards the exact center of the circle. Accurate position, velocity and especially yaw angle control are needed to accurately follow the desired flight plan with the desired attitude. Figure 13 shows the simulation results.

C. Entire flight envelope

The following flight simulation, see Fig. 14, shows a complete mission in which we evaluate all hybrid MAV flight capabilities through a vertical take-off from zero to ten meters of altitude followed by the hover-to-forward transition

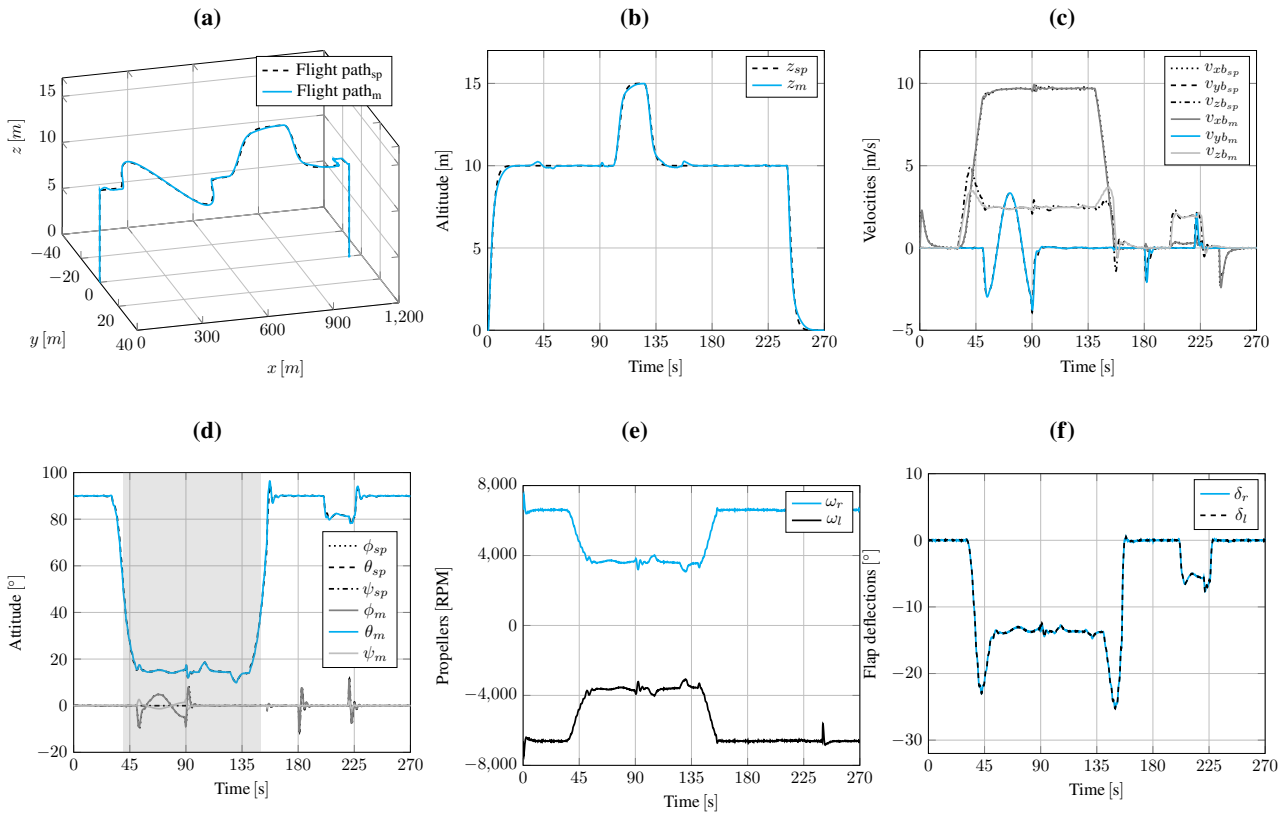

Fig. 14 Entire flight envelope simulation in relatively calm flight conditions. On the top, from left to right: the 3D flight path, altitude and velocities in the body coordinate system. On the bottom: attitude, propeller speeds and flap deflections.

with a position tracking in the $xy-plane$ and an altitude change in forward flight. Then, the forward-to-hover transition is performed with a position tracking in hovering flight. The flight simulation ends with a vertical landing. The complete 3D flight path is presented in the Fig. 14a. The controller assures the position tracking during the entire mission. As we can see in the Fig. 14b, the altitude presents small oscillations at 45 and 165 seconds of simulation which is acceptable for this MAV class. These oscillations are due to the fast variations of aerodynamic forces and moments that occur during the transition flight phases where the pitch angle changes resulting in significant variations in the angle of attack, see Fig. 14d. In the same figure, between 45 and 90 seconds of simulation, we can see the roll angle behaviour in charge of reach the desired east position in forward flight. Similarly, between 180 and 215 seconds of simulation, the yaw behaviour in charge of reach the east position in hovering flight. Figure 14c presents the velocities in the body coordinate system and the actuator dynamics, respectively, the propeller rotations and the flap deflections are shown in the Fig. 14e and Fig. 14f.

VII. Preliminary Flight Experiments

We present in this section first experimental flight results with MFC algorithms for tail sitter MAV in outdoor and indoor environments. Two indoor experiments were performed in the *ENAC's flying arena* which has a flight volume of about 10x10x10 meters, see Fig. 15. The entire flight domain is covered by *Optitrack* cameras that informs in real time the DarkO's attitude orientation and position. However, in these experiments, we analyse only the attitude control loop by using the *Optitrack* cameras for heading measurements. For the outdoor flight, a compass is used to obtain the heading orientation. The entire attitude is computed on-board at 500 Hz by a complementary filter algorithm that combines both accelerometer and gyroscope signals. The attitude setpoints are set externally by the pilot from a RC transmitter.

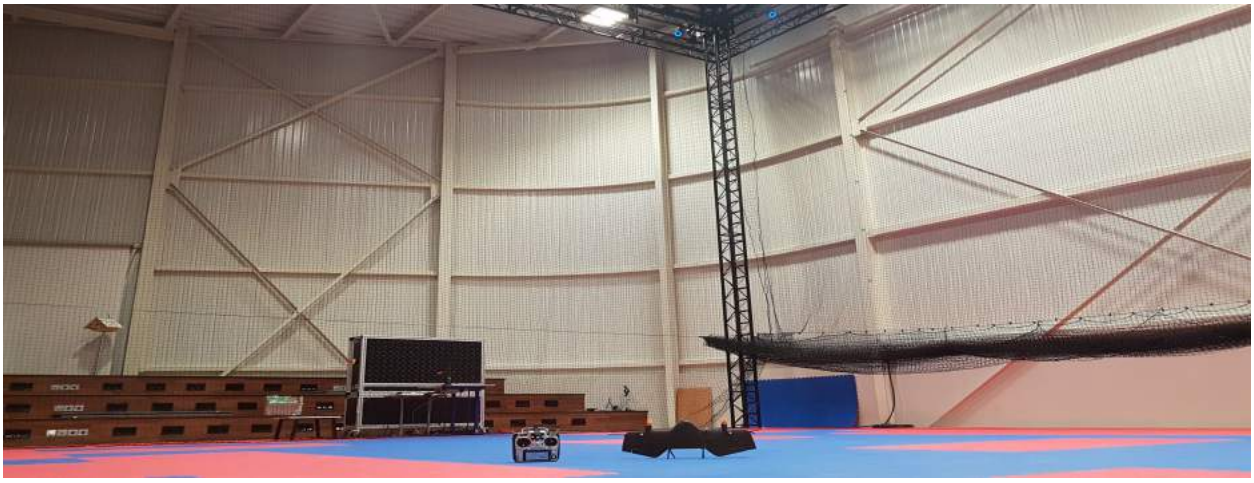

Fig. 15 Dark0 Tail Sitter MAV at rest in the *ENAC's flying arena* showing two of sixteen *Optitrack* cameras in the top and the *WindShape* wind generator in the background.

A. Indoor transitioning flights

The first indoor experiment show the adaptation properties of the controller during flights with high incidence angle variations, see Fig. 16. The pitch angle trajectories do not remain on angles below 20 degrees, for a long time, in forward flight due to size limitation of the flight area. In order to avoid the collision with the protective nets, the pilot imposes a pitch angle setpoint of around 90° bringing the DarkO back to stationary flights in hovering flight phase. The nonlinear cancelation term (30) and (34), has fast adaptation properties that keeps the correct commands up-to-date for the entire flight envelope ensuring the DarkO attitude stabilization despite the fast variations of aerodynamic forces and moments. This is a particularly powerful feature of this control architecture in the sense that it can, in principle, adjust the control output in order to achieve desired dynamics for an unknown nonlinear system.

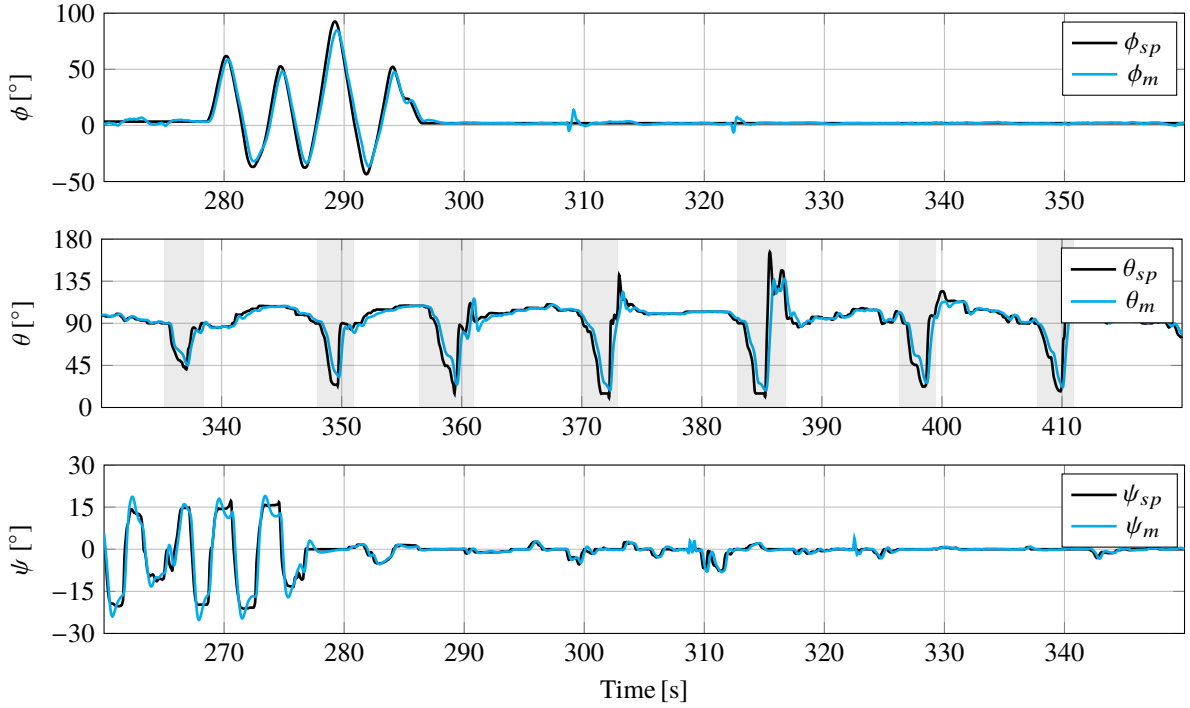

Fig. 16 Attitude stabilization during indoor flights with fast transitioning flights.

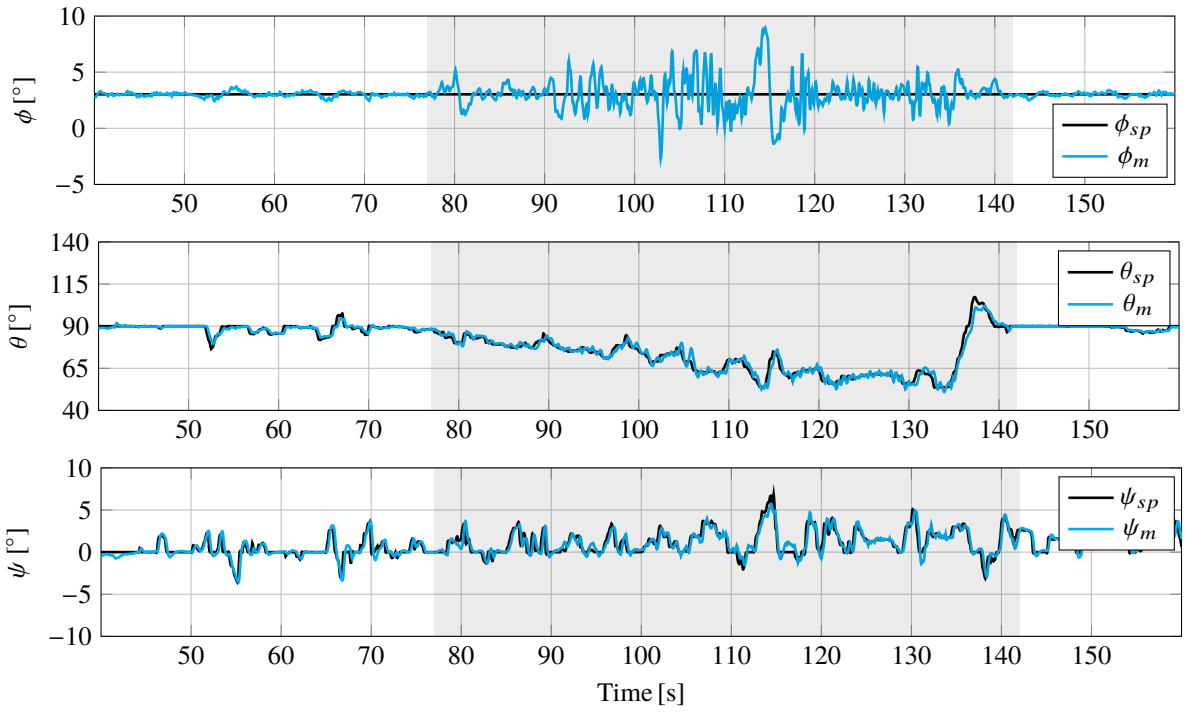

Fig. 17 Experimental transitioning flight faced to the *WindShape* small wind generator.

The second flight experiment analyzes the disturbance rejection properties of the model-free control algorithm for attitude stabilization during indoor transitioning flight. For this experiement, we reproduce the conditions that are met by MAV in outdoor environments using the *WindShape* open type wind tunnel*. DarkO starts the mission in hovering flight mode faced to the *WindShape* and, according to increase of the wind speed from zero to 9 m/s, the pilot continually updates the pitch angle to perform the transition with the objective of counteract and reduce major wind influences on the position of the DarkO, while maintaining its heading to stay upwind. The stabilized attitude angles are presented in the Fig. 17. The shaded area highlights the roll angle (ϕ) oscillations as well as the flight domain where the pitch angle (θ) decreases by approaching to the forward flight. The roll angle is controlled by asymmetric flap deflections, and the pitch angle by symmetric flap deflections. Thus, for high incidence angles, the roll oscillations of around 8° can be explained by the coupled dynamics between these axes. We can reduce the dynamic dependencies of one axis on the other by optimizing the MFC parameters in order to improve the DarkO performance, particularly during transitioning flights with wind disturbances.

B. Outdoor transitioning flights

The objective of this flight experiment is to validate the attitude control loop performance in outdoor flight conditions, in particular the disturbance rejection properties, and compare the results with the previous indoor flight experiment. Figure 18 shows the attitude behaviour for the outdoor flight experiment. We analyse the tail sitter MAV flight modes 2, 3, and 4 as described in the Fig. 1. The DarkO starts the experiment in the hovering flight phase and, according to pitch angle setpoints from RC transmitter, different transitioning flights are performed, from both hover-to-forward and forward-to-hover. The detailed pitch angle result is shown in the Fig. 19, we can observe a smooth and continuous stabilized flight transition. The roll oscillations highlighted in the indoor flight were not observed on this flight. Yet, we used exactly the same MFC parameters.

*www.windshape.ch

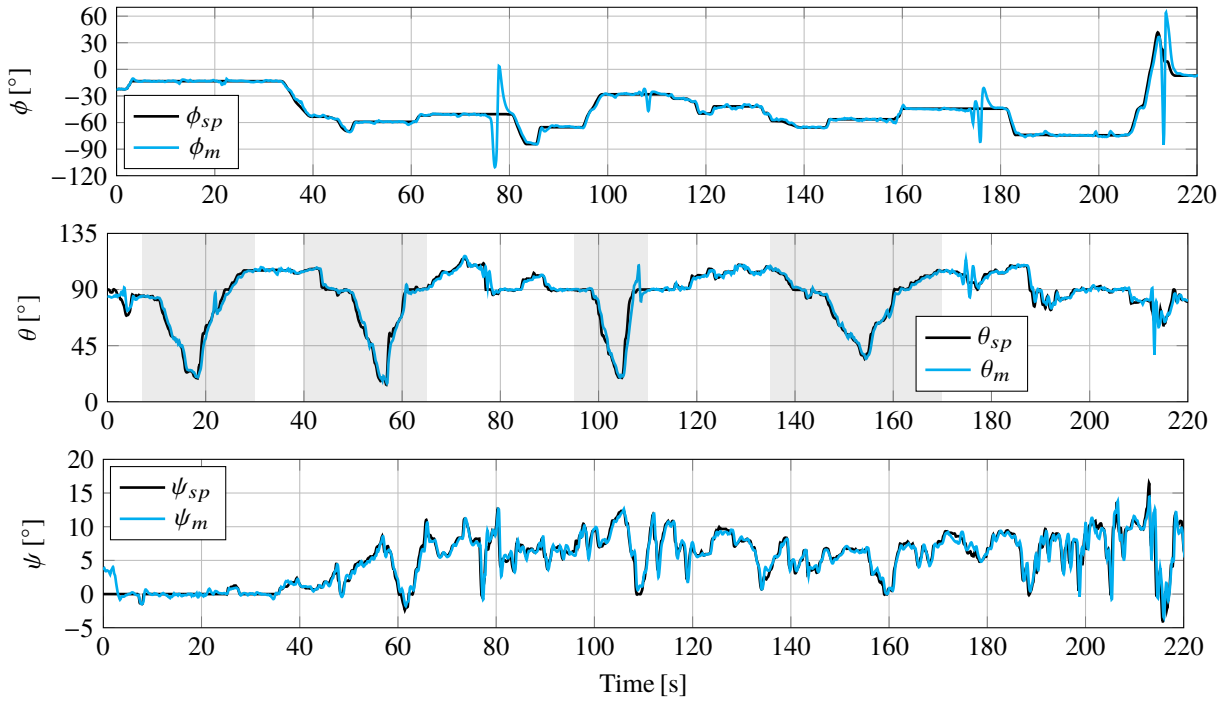

Fig. 18 Attitude stabilization during outdoor flight experiment.

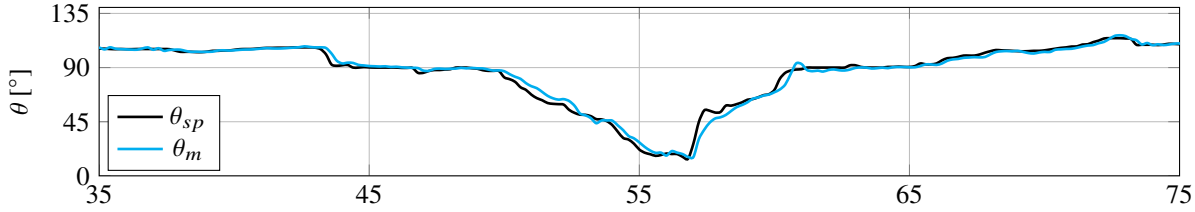

Fig. 19 Pitch angle result for $t \in [35; 75]$ seconds during outdoor flight experiment.

VIII. Conclusion

We have designed a control architecture based on model-free control algorithms to tackle the entire flight envelope of tail sitter MAVs. Flight simulations were performed in order to validated the interactions between each control block covering their wide flight domain. The proposed control approach provides, according to flight simulation results, high performance for position tracking, velocity control, and attitude stabilization without neither gain scheduling methods nor any prior knowledge of tail sitter MAV parameters. Because unmodeled dynamics are measured at the controller input, no complex modeling processes are needed which facilitates its implementation in new MAVs. We also examined the attitude control loop performance during experimental flights in outdoor and indoor environments which highlighted the disturbance rejection properties of such a controller. The most obvious finding to emerge from this study is the easy implementation of the MFC algorithm to different hybrid MAV platforms. However, this finding must be verified by implementing the proposed controller in different MAVs with different physical characteristics. Additionally, we would like to investigate the guidance challenges involving tail sitter MAVs in real flight conditions.

Acknowledgments

Authors would like to thank Xavier Paris and Michel Gorraz for their support during flight experiments.

References

[1] Santos, M. A., Cardoso, D. N., Rego, B. S., Raffo, G. V., and Esteban, S., "A Discrete Robust Adaptive Control of a Tilt-rotor UAV for an Enlarged Flight Envelope," *IEEE 56th Annual Conference on Decision and Control (CDC)*, Melbourne, Australia, December 2017, pp. 5208–5214.

[2] P. Hartmann, C. M., and Moormann, D., "Unified Velocity Control and Flight State Transition of Unmanned Tilt-Wing Aircraft," *Journal of Guidance, Control, and Dynamics*, Vol. 40, No. 6, June 2017, p. 1348–1359.

[3] H. Gu, Z. L.-S. S., X. Lyu, and Zhang, F., "Development and Experimental Verification of a Hybrid Vertical Take-Off and Landing (VTOL) Unmanned Aerial Vehicle(UAV)," *International Conference on Unmanned Aircraft Systems (ICUAS)*, Miami, FL, USA, June 2017, pp. 160–169.

[4] Flores, A., de Oca, A. M., and Flores, G., "A simple controller for the transition maneuver of a tail-sitter drone," *IEEE Conference on Decision and Control (CDC)*, Miami Beach, FL, USA, December 2018, pp. 4277–4281.

[5] K. Chinwicharnam, J.-M. M., D. Gomez Ariza, and Chinnapat, T., "Aerodynamic Characteristics of a Low Aspect Ratio Wing and Propeller Interaction for a Tilt-Body MAV," *International Journal of Micro Air Vehicles*, Vol. 5, No. 4, 2013, pp. 245–260.

[6] Bronz, M., Smeur, E. J. J., de Marina, H. G., and Hattenberger, G., "Development of A Fixed-Wing mini UAV with Transitioning Flight Capability," *35th AIAA Applied Aerodynamics Conference, AIAA AVIATION Forum*, 2017, pp. 1–14.

[7] Bilodeau, P.-R., and Wong, F., "Modeling and control of a hovering mini tail-sitter," *International Journal of Micro Air Vehicles*, Vol. 2, 2010, pp. 211–220.

[8] Hochstenbach, M., Notteboom, C., Theys, B., and Schutter, J. D., "Design and Control of an Unmanned Aerial Vehicle for Autonomous Parcel Delivery with Transition from Vertical Take-off to Forward Flight - VertiKUL, a Quadcopter Tailsitter," *International Journal of Micro Air Vehicles*, Vol. 7, No. 4, 2015, pp. 395–405.

[9] Lustosa, L. R., Defaÿ, F., and Moschetta, J.-M., "Longitudinal study of a tilt-body vehicle: modeling, control and stability analysis," *International Conference on Unmanned Aircraft Systems (ICUAS)*, Denver, Colorado, USA, June 2015, pp. 816–824.

[10] Kita, K., Konno, A., and Uchiyama, M., "Transition between Level Flight and Hovering of a Tail-Sitter Vertical Takeoff and Landing Aerial Robot," *Advanced Robotics*, Vol. 24, No. 5-6, April 2012, pp. 763–781.

[11] Silva, N. B. F., Fontes, J. V. C., Inoue, R. S., and Branco, K. R. L. J. C., "Dynamic Inversion and Gain-Scheduling Control for an Autonomous Aerial Vehicle with Multiple Flight Stages," *Journal of Control, Automation and Electrical Systems*, Vol. 29, No. 3, June 2018, pp. 328–339.

[12] Saeed, A. S., Younes, A. B., Cai, C., and Cai, G., "A survey of hybrid Unmanned Aerial Vehicles," *Progress in Aerospace Sciences*, Vol. 98, April 2018, pp. 91–105.

[13] Ritz, R., and D'Andrea, R., "A global controller for flying wing tailsitter vehicles," *IEEE International Conference on Robotics and Automation (ICRA)*, Singapore, May 2017, pp. 2731–2738.

[14] Knoebel, N. B., and McLain, T. W., "Adaptive quaternion control of a miniature tailsitter uav," *American Control Conference (ACC)*, Seattle, Washington, USA, June 2008, pp. 2340 – 2345.

[15] Jung, Y., and Shim, D. H., "Development and application of controller for transition flight of tail-sitter uav," *Journal of Intelligent & Robotic Systems*, Vol. 65, No. 1-4, January 2012, pp. 137–152.

[16] Hajiloo, A., and Rodrigues, L., "Modeling and Backstepping Control of Under-Actuated Spherical UAV," *IEEE Conference on Control Technology and Applications (CCTA)*, Kohala Coast, Hawaii, August 2017, pp. 2069–2074.

[17] Li, Z., Zhou, W., Liu, H., Zhang, L., and Zuo, Z., "Nonlinear Robust Flight Mode Transition Control for Tail-Sitter Aircraft," *IEEE Access*, Vol. 6, October 2018, pp. 65909–65921.

[18] Smeur, E. J. J., Bronz, M., and de Croon, G. C. H. E., "Incremental control and guidance of hybrid aircraft applied to the Cyclone tailsitter UAV," 2018 (Unpublished).

[19] Pucci, D., Hamel, T., Morin, P., and Samson, C., "Nonlinear feedback control of axisymmetric aerial vehicles," *Automatica*, Vol. 53, March 2015, pp. 72–78.

[20] Pucci, D., Hamel, T., Morin, P., and Samson, C., "Nonlinear Control of Aerial Vehicles Subjected to Aerodynamic Forces," *IEEE Conference on Decision and Control (CDC)*, Florence, Italy, December 2013, pp. 4839–4846.

[21] Wang, W., Zhu, J., Kuang, M., and Zhu, X., "Adaptive Attitude Control for a Tail-sitter UAV with Single Thrust-vectored Propeller," *IEEE International Conference on Robotics and Automation (ICRA)*, Brisbane, Australia, May 2018, pp. 6581–6586.

[22] Fliess, M., and Join, C., "Model-free control," *International Journal of Control, Taylor & Francis*, Vol. 86, No. 12, July 2013, pp. 2228 – 2252.

[23] Join, C., Bernier, J., Mottelet, S., Fliess, M., Rechdaoui-Guérin, S., Azimi, S., and Rocher, V., "A simple and efficient feedback control strategy for wastewater denitrification," *20th World IFAC Congress*, 1, Vol. 50, Toulouse, France, July 2017, pp. 7657–7662.

[24] Rodriguez-Fortun, J. M., Rotella, F., Alfonso, J., Carrillo, F. J., and Orús, J., "Model-free control of a 3-DOF piezoelectric nanopositioning platform," *52nd IEEE Conference on Decision and Control (CDC)*, Florence, Italy, December 2013, pp. 342–347.

[25] Bara, O., Fliess, M., Join, C., Daye, J., and Djouadi, S. M., "Toward a model-free feedback control synthesis for treating acute inflammation," *Journal of Theoretical Biology, Elsevier*, Vol. 448, No. 7, July 2018, pp. 26–37.

[26] Join, C., Robert, G., and Fliess, M., "Model-Free Based Water Level Control for Hydroelectric Power Plants," *IFAC Conference on Control Methodologies and Technology for Energy Efficiency*, 1, Vol. 43, Vilamoura, Portugal, March 2010, pp. 134–139.

[27] Abouaïssa, H., Fliess, M., and Join, C., "Fast parametric estimation for macroscopic traffic flow model," *17th IFAC World Congress*, Seoul, South Korea, July 2008, pp. 13040–13045.

[28] Chand, A. N., Kawanishi, M., and Narikiyo, T., "Non-linear Model-free Control of Flapping Wing Flying Robot using iPID," *IEEE International Conference on Robotics and Automation (ICRA)*, Stockholm, Sweden, May 2016, pp. 2930–2937.

[29] Younes, Y. A., Drak, A., Noura, H., Rabhi, A., and Hajjaji, A. E., "Robust Model-Free Control Applied to a Quadrotor UAV," *Journal of Intelligent & Robotic Systems*, Vol. 84, No. 1-4, December 2016, pp. 37–52.

[30] Lustosa, L. R., Defaÿ, F., and Moschetta, J.-M., "Global Singularity-Free Aerodynamic Model for Algorithmic Flight Control of Tail Sitters," Vol. 42, No. 2, February 2019, pp. 303–316.

[31] Drela, M., "XFOIL: An Analysis and Design System for Low Reynolds Number Airfoils," *Conference on Low Reynolds Number Airfoil Aerodynamics*, University of Notre Dame, June 1989.

[32] Chahl, J. S., Jain, L. C., Mizutani, A., and Sato-Ilic, M., *Innovations in Intelligent Machines-1, pp. 181*, Springer-Verlag Berlin Heidelberg, July 2007.

[33] Martin, P., and Salaun, E., "Design and implementation of a low-cost observer-based attitude and heading reference system," *Control Engineering Practice*, Vol. 18, No. 7, July 2010, pp. 712–722.